Effect of copper on calcium-modified alumina-supported cobalt catalysts towards Fischer–Tropsch synthesis

Sudip Maity[1,*], Olusola O. James[1,2,3], Biswajit Chowdhury[2] and Aline Auroux[4]

[1]Liquid Fuels Section, Central Institute of Mining and Fuels Research (DC), Dhanbad 828 108, India
[2]Applied Chemistry Department, Indian School of Mines, Dhanbad 828 108, India
[3]Chemistry Department, Covenant University, Canaan Land, Ota, Ogun State, Nigeria
[4]Institute de Rechereches sur la Catalyse et l'Environnement de Lyon, UMR 5256, CNRS/Universite Lyonl, France

The present study reports the possibility of using copper as a low-cost reduction promoter in cobalt-based Fischer–Tropsch (FT) catalysts. Adsorption behaviour of CO and H_2 on alumina-supported Co and Co–Cu catalysts has been examined. Amount of CO and H_2 desorption and temperature of desorption are used to gain insights about the performance of the catalysts. Presence of Cu alters CO and H_2 adsorption on Co–alumina catalyst. Modification of alumina with Ca enhances Co dispersion and the amount of CO adsorbed. However, increase in the amount of CO adsorbed does not translate into increase in CO conversion. The Co–Cu-based catalysts display higher amount of H_2 adsorbed and higher CO desorption temperature. The latter is at the expense of the amount of CO adsorbed for low CO conversion resulting in lower activity for FT synthesis. The catalysts display high selectivity towards oxygenates. The high CO adsorption strength on Co–Cu-based catalysts is rationalized in terms of synergistic interaction of CO with cobalt particles through carbon atom and copper particles through oxygen atom.

Keywords: Adsorption, alumina, copper–cobalt catalysts, desorption.

AT present the transportation industry depends almost exclusively on petroleum-derived liquid fuels. There have been debates and anticipation about shortage of crude oil supply in the future[1]. This has brought about a renewed interest in the Fischer–Tropsch (FT) synthesis for obtaining hydrocarbons from other carbonaceous resources (coal, natural gas, biomass, etc.). FT technology is an indirect liquefaction process via syngas intermediate; depending on the starting carbonaceous resource, it is often called *X*-to-liquid (*X* = C – coal, G – natural gas, B – biomass, etc.)[2,3].

Catalyst development has been at the centre of FT technology. Iron and cobalt-based catalysts are used in commercial FT operations. Although iron is cheaper than cobalt, there is a general preference for cobalt catalysts for gas-to-liquid (GTL) process. The main design objective in the cobalt-based FT catalysts is to disperse and stabilize metallic cobalt nanoparticles on a support material. The catalysts are usually prepared by impregnation method. Solution of cobalt precursor (nitrate or acetate) is impregnated on the support, followed by calcination and reduction/activation prior to the FT synthesis. Higher dispersion of the cobalt nanoparticles is usually obtained with gamma alumina than with silica support materials. However, large portion of the impregnated cobalt precursor on gamma alumina usually forms cobalt phases that are unreduced at the catalyst activation temperature[4,5]. The unreduced cobalt phases constitute material lost since these are inactive for the hydrocarbon synthesis. In some commercial catalysts high cobalt loading is adopted in order to have sufficient active sites. Moreover, textural and reduction promoters are included in commercial FT cobalt catalysts to enhance the reduction of the cobalt phases. The textural promoters can be metal oxides or other materials that can minimize formation of the unreduced cobalt phases as well as prevent sintering of the active sites. The textural promoter can also have an influence on the FT activity and product selectivity of the catalyst[6–8]. For instance, CaO promotion of Co/Al_2O_3 has shown to increase the FT activity and improve C_{5+} selectivity of the catalyst[9,10].

The reduction promoters are platinum group metals (PGM). Although the percentage composition of a PGM in a commercial cobalt-based FT catalyst is usually ≤ 1%, they account for ~ 50% of the catalysts cost. FT syncrude is characterized by its high content of linear hydrocarbons and choice of promoters for cobalt-based catalysts for GTL plants is usually targeted to minimize methane and maximize C_{5+} selectivity. Although ruthenium ranks higher than cobalt in FT and C_{5+} selectivities, scarcity and high cost of Ru make its use in Ru-based FT catalyst unsustainable. When employed as a promoter, Ru enhances activity and C_{5+} selectivity of cobalt-based catalysts. While straight run middle distillate range hydrocarbons from syncrude from such catalysts will have high cetane

*For correspondence. (e-mail: sudip_maity@yahoo.com)

number, the gasoline range hydrocarbons will have low octane rating. Low molecular weight alcohols and oxygenates are octane boosters in automotive fuels[11,12]. In addition to the potential of copper as a lower cost-reduction promoter for cobalt FT catalyst, it can also promote alcohol and oxygenate selectivity. However, there are only few reports on the use of an copper as an alternative to PGM in cobalt FT catalysts[13–16]. Also, there are contrasting reports on the effect of copper promotion on the FT activity and selectivity of the catalysts. Since adsorption is a key elementary step in heterogeneous catalysed reactions, in the present article, we report temperature programmed desorption (TPD) technique to study CO and H_2 adsorption on Cu-promoted and unpromoted Co/Al_2O_3 catalyst. We have used polyol modified impregnation technique as an easy scale method for achieving high dispersion of metal nanoparticles on a support material. We also study the effect of Cu and CaO promotion on Co/Al_2O_3 catalyst. The catalysts have also been characterized using X-ray diffraction (XRD), X-ray photoelectron spectroscopy (XPS), hydrogen-temperature programmed reduction (H_2-TPR), O_2-titration, and we have attempted to correlate adsorption behaviour of CO and H_2 on the catalysts with their performance for FT synthesis.

Experiment

Catalyst preparation

CaO-modified alumina was prepared by wet impregnation of γ-alumina (Sasol GmbH, Germany, extrudates, BET surface area 181 $m^2\ g^{-1}$; pore volume: 0.49 $cm^3\ g^{-1}$) with calcium nitrate at 7.5 mol% loading. CaO-modified and unmodified alumina samples were calcined at 550°C for 6 h. The supports were then impregnated with cobalt and copper metal nitrate solution containing glycerol (M^{n+}/glycerol mole ratio 4) at 20 mol% Co loading for all the catalysts and 4 mol% Cu loading for the promoted catalysts. The metal ion(s) loaded on supports were dried at 110°C overnight and calcined at 350°C for 6 h.

Catalyst characterization

N_2 physisorption: Specific surface area of catalysts was measured using Chemisorb 2720 (M/s Micromeritics, USA). The surface area was determined using the Brunauer–Emmett–Teller (BET) equation by the single-point method from the amount of desorbed nitrogen after physisorption at liquid-nitrogen temperature.

X-ray diffraction: XRD of the catalysts was recorded at room temperature on a D8 ADVANCE (BRUKER AXS, Germany) diffractometer using CuK_α radiation with parallel beam (Gobel Mirror). The catalysts were ground to fine powder prior to measurement. The scans were recorded in the 2θ range between 10° and 75° using step size of 0.02° and scan speed of 2s/step. Peaks were identified by search match technique using DIFFRAC^{plus} software (BRUKER AXS, Germany) with reference to the JCPDS database. The software TOPAS 3.0 from Bruker AXS (2005) was used for refinement of Co_3O_4 diffraction peak (311) located at $2\theta = 36.9°$ to determine the average crystallite size.

X-ray photoelectron spectroscopy: XPS analysis of the catalysts was carried out with a PHI-5500 spectrometer with AlK_α radiation (1253.6 eV). The energy was calibrated with a C 1s peak.

Temperature programmed reduction: TPR profiles of the samples were obtained with ChemiSorb 2720 (M/s Micrometrics, USA) equipped with a TCD detector. The TPR profiles were obtained by reducing the catalyst samples by a gas mixture of 10% H_2 in Ar with a flow rate of 20 ml/min, while the temperature was increased from ambient to 800°C at a rate of 10°C/min.

Reducibility: Reducibility of the supported catalysts was determined by O_2-titration. The catalysts were first reduced at 350°C for 8 h with pure hydrogen and reoxidized with 5% O_2 in He at the same temperature using pulse chemisorption technique. The percentage of reducibility (R_0) was calculated by assuming complete re-oxidation of Co to Co_3O_4 according to the chemical equation: $3Co + 2O_2 \rightarrow Co_3O_4$.

$$\%R_0 = \frac{\text{No. of moles of } O_2 \text{ uptake}}{\text{Stochiometric no. of moles of } O_2} \times \frac{3}{2} \times 100. \quad (1)$$

Temperature programmed desorption: TPD was carried out by first reducing a catalyst with H_2 at 350°C for 8 h. For H_2-TPD, the catalyst was cooled under hydrogen flow to and maintained at 100°C for 30 min. Then the catalyst surface was purged for 1 h with Ar flow before the temperature was raised from 100°C to 1000°C at 10°C/min. For CO-TPD, the catalysts were reduced with H_2 at 350°C for 8 h, gas flow was switched to He and temperature is raised to 400°C at rate of 10°C/min and then kept at 400°C for 30 min before cooling to ambient temperature to eliminate adsorbed H_2 from the catalyst surface. CO adsorption was carried out at 100°C using 5.2% CO in He. Then the TPD profile was obtained by a temperature programme at a rate of 10°C/min under He flow with a flow rate of 20 ml/min from ambient to 1000°C temperature.

Catalyst tests

The reactor set-up of the FT synthesis experiment is shown in Figure 1. Five millilitres of each catalyst was

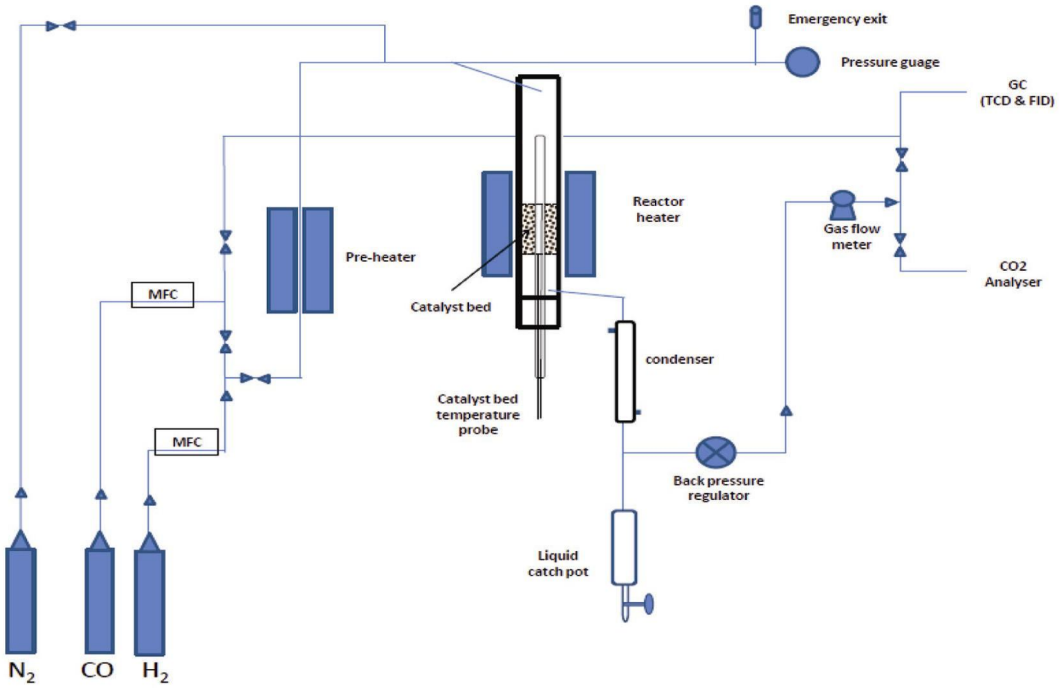

Figure 1. Fischer–Tropsch (FT) reactor set-up.

loaded in the reactor. Two thermocouple probes were fixed at the upper and lower of catalyst bed temperature to monitor the reaction temperature. After loading the catalyst, the leak test was performed for each experiment by feeding the reactor with N_2 up to a pressure of 10 bar. The set-up was considered leak-proof when the pressure level remained unchanged for at least 48 h. Then catalyst was reduced under H_2 at 350°C for 10 h. After reduction, the reactor was cooled to the reaction temperature of 220°C. The preheater and the feed gas line were kept at a temperature of 170°C. The F–T synthesis runs were conducted with H_2/CO ratio of 2 : 1, gas hourly space velocity (GHSV) of 600 h^{-1} and 220°C temperature and 20 bar pressure. Condensed products were collected in the liquid catch pot, while the remaining gases exited through the gas flow meter. Condensed products separated into fractions oil and aqueous phase. Wax product accumulated below the catalyst bed and was collected when the reactor was opened at the end of each experiment. CO_2 was analysed using Simens Ultramart CO_2 analyser. The exit gases were continuously monitored by a GC (Model-GC 1000; Make: M/s Chemito Technologies Ltd, India) equipped with TCD and FID detectors. The oil portion of the accumulated liquid products collected from the catch pot were analysed for their hydrocarbon spectrum with GC-SIMDIST.

Results

XRD and XPS

XRD peaks of unloaded and metal-loaded gamma alumina were examined (Figure 2 *a*) which revealed that the crystalinity of alumina was unaffected by CaO loading. The loaded CaO and CuO were well-dispersed on the alumina. This may be due to pH and cobalt ion catalysed transformation of the alumina phase during cobalt impregnation[17,18]. A peak at $2\theta = 36.9°$ was prominent in all the XRD patterns of the four catalysts (Figure 2 *b*). The peak is typical of CoO and Co_3O_4 phases.

XPS analysis indicated that surface cobalt, copper and calcium species were in the +2 oxidation state. This suggests that CoO is the probable cobalt phase on the catalysts surface. However, presence of other cobalt phases like Co_3O_4 cannot be ruled out. Hence, CoO_x ($1 \le x \le 1.5$) was used to designate the cobalt phases in the catalysts. XPS showed lower surface concentration of cobalt in CoO_x–CuO/Al_2O_3 compared to that of Co/Al_2O_3 (Tables 1 and 2).

TPR and reducibility

The TPR profiles of the catalysts are presented in Figure 3. The Cu-promoted catalysts displayed a single reduction peak at lower temperature compared to the unpromoted counterparts. The unpromoted catalysts also have a second broad reduction peak at 400–800°C. In a separate study we have found that analysis of the area under the TPR profiles can provide a reliable estimate of the reducibility of the cobalt phase in an unpromoted Co/Al_2O_3 catalyst. We have determined the reducibility of the catalysts from TPR profile and compared with that obtained by pulse O_2-titration experiment. The O_2-titration method gave lower reducibility value for CoO_x–CuO/Al_2O_3

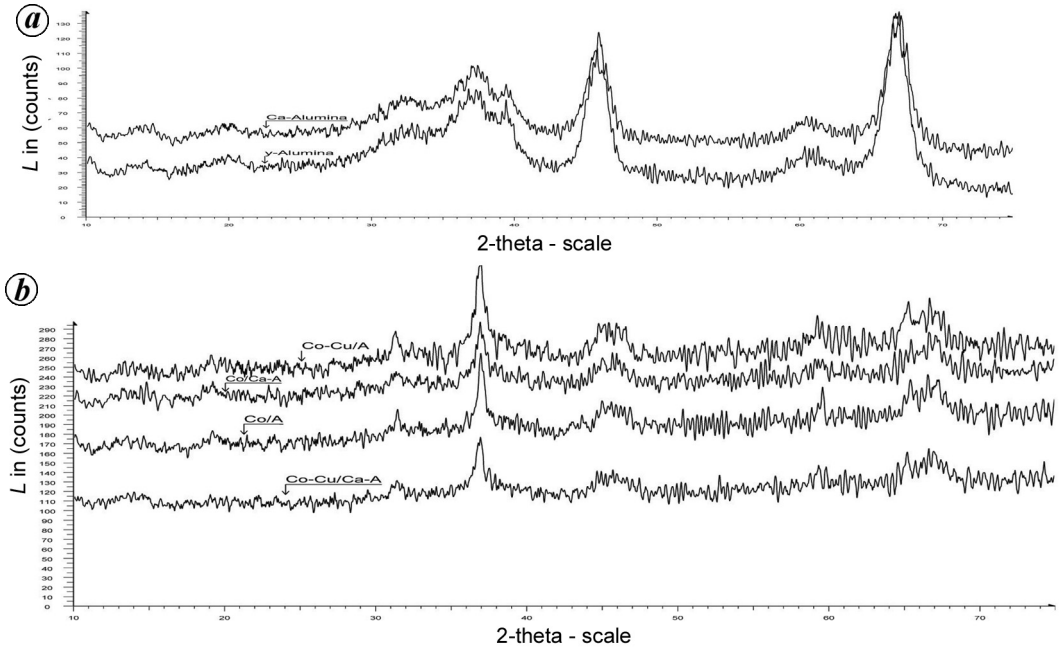

Figure 2. Diffractograms of (***a***) CaO-modified and unmodified γ-alumina and (***b***) catalysts.

Table 1. Binding energy of the catalyst components

	XPS binding energy			
Catalyst	Al $2p_{3/2}$	Co $2p_{3/2}$	Cu $2p_{3/2}$	Ca $2p_{3/2}$
Co/Al_2O_3	74.50	781.20		
$Co–Cu/Al_2O_3$	74.50	781.00	933.30	
$Co/Ca–Al_2O_3$	74.50	780.70		347.30
$Co–Cu/Ca–Al_2O_3$	74.50	780.40	933.60	347.40
Probable surface species	Al_2O_3	Co^{2+} (CoO)	Cu^{2+} (CuO)	$Ca(NO_3)_2$

Table 2. Surface composition of the catalyst components

	Surface composition				Relative ratio of the surface elements			
Catalyst	Al	Co	Cu	Ca	Co/Al	Ca/Al	Cu/Al	Cu/Co
CoO/Al_2O_3	38.32	0.71			0.019			
$CoO–CuO/Al_2O_3$	33.07	0.52	0.19		0.016		0.006	0.365
$CoO/Ca–Al_2O_3$	35.89	1.17		1.46	0.033	0.041		
$CoO–CuO/Ca–Al_2O_3$	33.71	1.11	0.27	1.37	0.033	0.041	0.008	0.243

compared to the value obtained from TPR profile. This may be due to inhibition to re-oxidation of the reduced cobalt nanoparticles.

BET surface area and crystallite size

BET surface area and crystallite size of the cobalt phase are given in Table 3. BET surface area of the catalysts decreased with increasing metal loading on the alumina. Crystallite size of the cobalt phase determined from the XRD peak at $2\theta = 36.9°$ using Scherrer equation ($L = k\lambda/\beta\cos\theta$, where L is the crystallite size; K a dimensionless shape factor close to unity; λ the X-ray wavelength; β the line broadening at half the maximum intensity (FWHM), in radians and θ is the Bragg angle) showed that the use of polyol improved dispersion of the cobalt phase. The presence of promoters (Cu and Ca phases) further enhanced dispersion of cobalt phase. The influence of the two promoters (Cu and Ca) resulted in about the same crystallite size of the cobalt phase in the respective catalysts.

Temperature programmed desorption

Figure 4 shows the CO-TPD profiles of the supports and catalysts. The amount of CO adsorbed by the catalysts followed the same trend as the acidic sites distributions (Figure 5) on the catalysts. Adsorptions studies were carried out on the supports in order to delineate between interaction of the adsorbed molecule with metal site and the support. The CO desorption profiles of the catalysts were markedly different from those of the supports. CO desorption began at > 220°C and < 160°C on the supports and catalysts respectively, showing that CO adsorbed more strongly on the support than on the catalysts (Figure 4). CO desorbed at higher temperature on Cu-promoted catalysts than on their unpromoted counterparts. But the amount of desorbed CO on the Cu-promoted catalysts was lower compared to those of their unpromoted counterparts (Figure 5).

Figure 6 shows the H_2-TPD profiles of the supports and catalysts. The figure reveals similar H_2-TPD profiles for the catalysts. However, Figure 7 shows varied amount of desorbed hydrogen for the catalysts. The amount of desorbed H_2 from unmodified alumina was higher on the support than on the catalysts. Also, the amount of desorbed hydrogen was higher in Cu-promoted catalysts, while Ca-containing catalysts displayed lower amount of desorbed hydrogen (Figure 7).

FT-synthesis

The TCD and Flame Ionization Detector (FID) analysis of the reactor exit gas is presented in Table 4. Exit H_2/CO ratio of the promoted catalysts was lower than that of the unpromoted catalyst. This implies that the promoted catalysts display higher H_2/CO usage ratio compared to the unpromoted catalyst. Usually high H_2/CO usage ratio is an indication of high hydrogenation activity and high selectivity to methane and gaseous products. However, the results presented in Table 4 show that the H_2/CO usage ratio of the promoted catalysts does not reflect in their C1–C4 selectivities. While reason(s) for this unusual

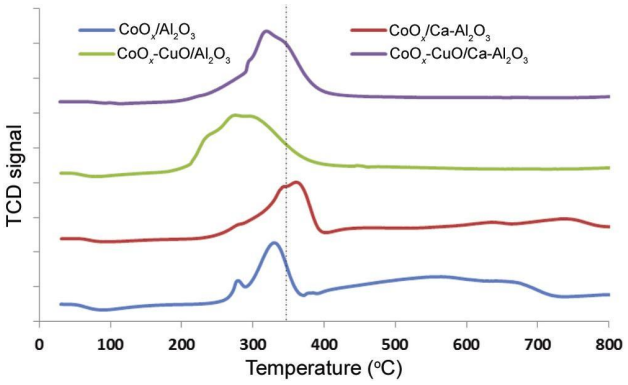

Figure 3. H-TPR profiles of the catalysts.

Table 3. Crystallite size of the catalysts

Entry	Catalyst	Crystallite of cobalt phase size (nm)	BET surface area (m^2/g)
1	CoO_x/Al_2O_3*	27.6	
2	CoO_x/Al_2O_3	19.2	90
3	CoO_x–CuO/Al_2O_3	11.6	87
4	CoO_x/Ca–Al_2O_3	11.9	85
5	CoO_x–CuO/Ca–Al_2O_3	13.9	73

*Impregnation without addition of glycerol.

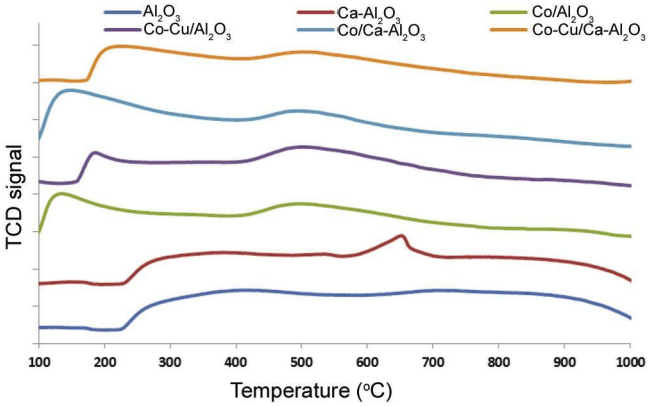

Figure 4. Desorption profiles of adsorbed CO on the supports and catalysts.

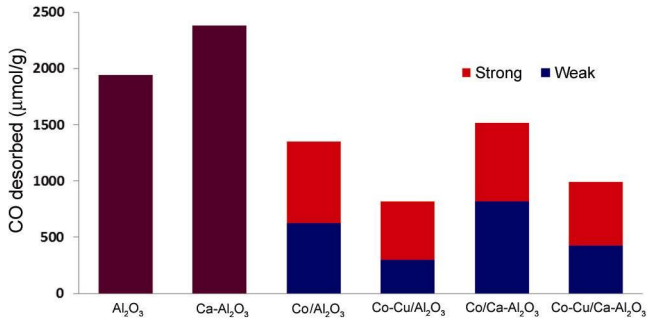

Figure 5. Site distribution of adsorbed CO on the catalysts.

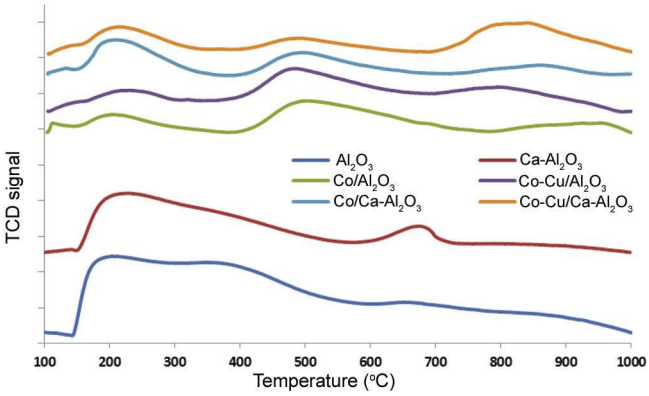

Figure 6. Desorption profiles of adsorbed H_2 on the supports and catalysts.

Table 4. Reactor exit gas composition

Gas	Catalyst			
	Co/Al_2O_3	$Co–Cu/Al_2O_3$	$Co/Ca–Al_2O_3$	$Co–Cu/Ca–Al_2O_3$
H_2	43.5	59.3	50.2	50.7
CO	20.4	36.4	36.6	44.0
CO_2	3.3	0.1	0.0	0.0
CH_4	22.4	2.9	7.9	2.6
C_2	3.9	0.5	1.9	0.9
C_3	4.2	0.5	1.1	1.2
C_4	2.3	0.3	1.1	0.6

Catalytic tests were performed at 220°C, 20 bar and $H_2/CO = 2$.

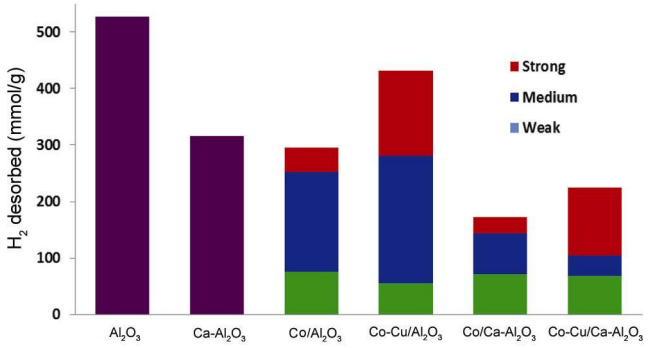

Figure 7. Site distribution of adsorbed H_2 on the catalysts.

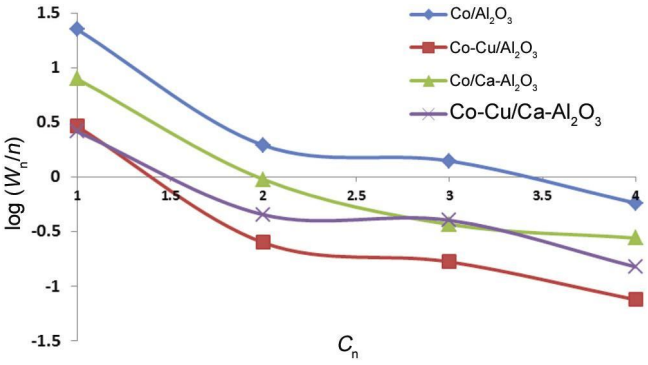

Figure 8. Mini-ASF plot for the catalysts using C_1 to C_4 selectivities depicting their unusual C_2 selectivity.

behaviour of the catalysts is not clear at present, it is observed that characteristic deviation in C_2 selectivity from Anderson–Schulz–Flurry (ASF) distribution that is typical of Fischer–Tropsch Synthesis (FTS) production spectrum is less apparent in the catalysts, especially the Ca-containing catalysts (Figure 8). It is also worth noting that CO_2 and CH_4 selectivities of the promoted catalysts are very low compared to that of the unpromoted catalysts. Presence of Ca and Cu promotion virtually suppresses CO_2 selectivity, but presence of Cu appears to have greater influence on the decrease of methane selectivity. This is contrary to the observation of Jacobs *et al.*[14], who reported increased methane and decreased C_{5+} selectivities in a copper-promoted Co/Al_2O_3 catalyst.

Discussion

Catalyst preparation method also has an impact on the cobalt phase dispersion. Although cobalt nitrate impregnation is generally found to give lower cobalt phase dispersions compared to other methods such as deposition precipitation and microemulsion, it is still the most common method used in commercial catalysts preparations because of its simplicity and easy scalability. Recent reports have shown that addition of an organic compound to the cobalt nitrate solution prior to impregnation can increase dispersion of cobalt on supports[19]. We modified the cobalt nitrate solution with glycerol to enhance dispersion of the cobalt phase the supports. As shown in Table 3 higher dispersion of cobalt phase was achieved with the addition of glycerol to the cobalt nitration solution compared to the one without glycerol. Similar enhancement of cobalt dispersion was achieved with sucrose by Ha *et al.*[20].

Although thermal decomposition of cobalt nitrate in air normally yields Co_3O_4 phase[21], it has been shown that Co_3O_4 can be reduced to CoO using glycerol at 320°C (ref. 22). Thus, in addition to enhancing the dispersion, glycerol also acts as a reducing agent for the reaction $Co_3O_4 \rightarrow CoO$, as indicated by the XPS results. The reaction $CoO \rightarrow Co$ accounts for the sole TPR peak in the Cu-promoted catalysts as well as the first sharp peak in the TPR profiles of the Cu-free catalysts[23]. The second broad peak in the TPR profiles of the Cu-free catalysts is attributed to reduction Co-Al hydrotalcite-like phases[4,6,24].

Interestingly, about the same crystallite size is obtained for $CoO_x–CuO/Al_2O_3$ and $CoO_x/CaO–Al_2O_3$. The enhanced dispersion of the cobalt phase in the catalysts is due to physical and/or chemical interactions with their respective supports. Copper is co-impregnated with cobalt, while calcium has been loaded prior to cobalt. Enhanced dispersion of cobalt phase in $CoO_x–CuO/Al_2O_3$ may also be due to inhibition of cobalt phase crystal growth by CuO acting as sandwich between cobalt phases. In the Ca-containing catalysts, alumina is impregnated with calcium nitrate and calcined at 550°C. At this temperature, $Ca(NO_3)_2$ decomposes to CaO. However, upon exposure to atmospheric condition and during the cobalt loading

step, CaO phase is prone to transformation to $CaCO_3$. Also there is a tendency of acid–base interaction $CaO/CaCO_3$ and cobalt [$CaO/CaCO_3 + Co(NO_3)_2 \rightarrow CoO/CoCO_3 + Ca(NO_3)_2$] leading back to $Ca(NO_3)_2$ phase.

The nature of CO adsorption on cobalt surface has been a subject of many studies, and it is generally agreed that CO adsorption on cobalt surface at room temperature is undissociative in a linear or bridged form[25]. Linear-type adsorbed CO desorbs at about 77°C, while bridge-type undergoes disproportionation reaction, $2CO \rightarrow C + CO_2$ at 167°C (refs 26, 27). In the present study, CO adsorption was carried out at 100°C, and programmed desorption also started at 100°C. Hence, the first peaks in the CO-TPD profiles of the catalysts were assigned to bridged-type adsorbed CO.

The amount of CO adsorbed on metal sites is a function of adsorption stoichiometry and metal dispersion. Cu–CO interaction is weaker than Co–CO in terms of strength and stoichiometry. As shown in Figure 5, decrease in the amount of CO adsorbed on the copper containing catalysts may be related to decoration effect of copper clusters on cobalt nanoparticles[28]. However, the observed higher CO desorption temperatures on copper containing catalysts is not consistent with normal Cu–CO interaction. Similar decrease in the amount of CO adsorbed has been observed on $Pd–Cu/SiO_2$ catalyst[29]. It has been shown through density function theory calculation that furfural is adsorbed on Cu/SiO_2 through carbonyl O in a g1(O)-aldehyde configuration. Copper alloy of Pd, Ni and Co was found to exhibit higher hydrogenation activity and selectivity for conversion of furfural to furfuryl alcohol[30,31]. The performance of the catalysts was explained in terms of synergistic adsorption of the carbonyl compound through O atom by copper and through the C atom by the alloy metals (Pd, Ni, Co). Strong molecular CO adsorption on Co^{2+} species has been proposed to account for alcohol selectivity in Co–Cu catalyst[32–34]. In the present study, copper containing catalyst showed higher reducibility than the copper-free counterpart, hence, stronger CO adsorption on the catalyst will be inconsistent with the presence of non-reducible cobalt species. A plausible explanation for the observed CO adsorption strength in the copper-containing catalysts is a synergistic interaction of CO with cobalt and copper through its carbon and oxygen atoms respectively. This adsorption behaviour of CO on the Co–Cu-based catalysts is strongly connected with the observed oxygenates selectivity of $Co–Cu/Al_2O_3$.

Co showed higher H_2 chemisorption capacity compared to Cu. But the adsorption capacity of the metals (Co, Cu) is an order of magnitude lower than that of γ-alumina. It appears that the H_2 adsorption capacities of the catalysts are largely due to the supports. Cu-support interface appeared to promote H_2 adsorption. In spite of the separate facile adsorption of CO and H_2 on the supports, they were not active for CO hydrogenation or C–C coupling. This may suggest that CO and H_2 adsorption on the supports is mutually exclusive or the phases of the support (Al and Ca) are not redox-active. CO adsorption requires either an acidic or a basic site; H_2 chemisorption requires a pair of acid–base sites. A recent report has implicated Al–O–CO units in the transition state involved in CO activation step of FT synthesis over γ-alumina-supported cobalt catalyst[35]. CO hydrogenation is not a facile process on γ-alumina because CO adsorption on γ-alumina surface may impair H_2 adsorption. However, γ-alumina may serve as hydrogen and CO reservoir for metal sites in γ-alumina-supported metal catalysts for syngas conversion.

The carbon number distribution of oil portions of the products is shown in Figure 9. All the Co-based catalysts showed similar positively skewed unimodal product distribution of hydrocarbons with modes occurring around $C_9–C_{13}$ for Co/Al_2O_3, $Co/CaO–Al_2O_3$ and $Co-Cu/CaO-Al_2O_3$ catalysts, whereas mode occurred at $C_{11}–C_{15}$ for $Co–Cu/Al_2O_3$ catalyst. The carbon number distribution of hydrocarbons from the catalysts followed ASF distribution till about C_{25}, after which the data curve deviated from the straight line. This kind of deviation for ASF distribution model has been widely reported. It is believed that such deviation is due to natural low diffusivity of the FTS products with increasing carbon number which contributes to decreasing tendency of desorption from the active sites of the catalysts.

Calculated chain growth probabilities (α values) of the catalysts from ASF plot (Figure 10) and a summary of the carbon number range product selectivity of the catalysts are presented in Table 5. The α values of product distribution for the catalysts decreased with increasing metal loading on γ-alumina. This coincides with increase of $C_5–C_7$ and decrease of $> C_{19}$ selectivities of the catalysts (except $Co–Cu/Al_2O_3$) with increasing metal loading on γ-alumina. From Table 2, it can be observed that the surface concentration of cobalt in the presence of the promoters suggests that the promoters inhibit or block the chain growth sites. The Cu promotion leads to increase in $> C_{19}$ selectivity and decrease in $C_5–C_7$ selectivity as evident from the product distribution for the catalysts Co/Al_2O_3 and $Co–Cu/Al_2O_3$ (Table 5). But the $C_8–C_{18}$ selectivity increases with increasing metal loading on γ-alumina.

The C_{5+} hydrocarbon distribution of the cobalt catalysts in terms of fuel classification is also presented in

Table 5. Summary of carbon number range product selectivity of the cobalt catalysts

Catalyst	$C_5–C_7$	$C_8–C_{18}$	$> C_{19}$	α-value
Co/Al_2O_3	9.9	66.6	22.6	0.84
$Co–Cu/Al_2O_3$	2.2	69.8	27.7	0.82
$Co/CaO–Al_2O_3$	12.3	70.5	16.5	0.81
$Co–Cu/CaO–Al_2O_3$	17.7	72.5	9.5	0.80

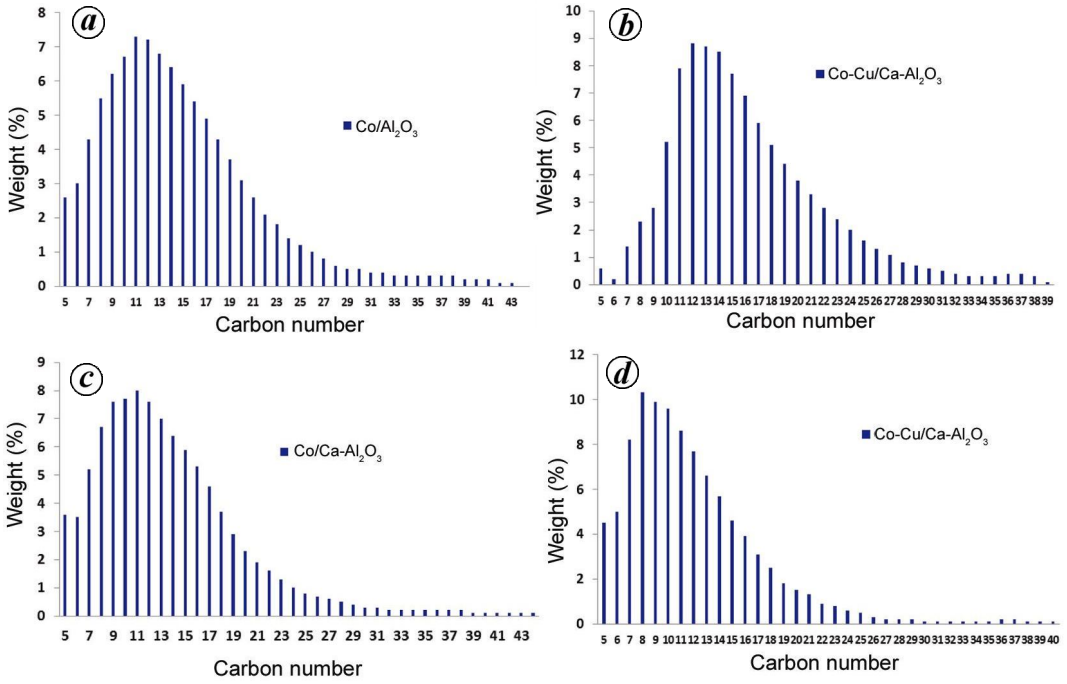

Figure 9. Product distribution of the oil portion of the liquid product of the catalysts. ***a***, Co/Al_2O_3; ***b***, $Co–Cu/Al_2O_3$; ***c***, $Co/Ca–Al_2O_3$; ***d***, $Co–Cu/Ca–Al_2O_3$.

Table 6. Accumulated non-gaseous products

Catalyst	Activity (g/g[cat]/h)	Non-gaseous products selectivity (%)				
		α-value		Oil	Aqueous	Wax
Co/Al_2O_3	0.043	19.2	0.84	23.9	75.9	0.2
$Co–Cu/Al_2O_3$	0.010	11.6	0.82	1.3	98.7	–
$Co/Ca–Al_2O_3$	0.015	11.9	0.81	14.7	85.3	–
$Co–Cu/Ca–Al_2O_3$	0.032	13.9	0.80	16.5	83.5	–

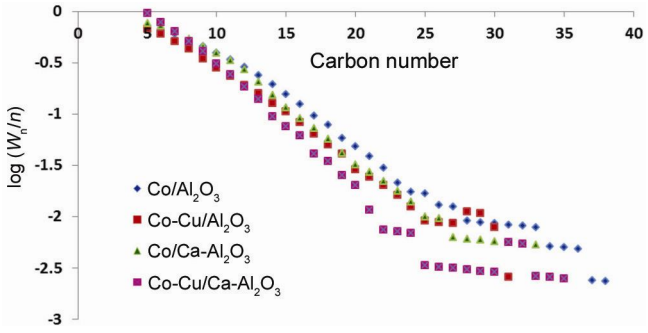

Figure 10. ASF plot of liquid hydrocarbon products of the cobalt catalysts.

Table 5. $Co–Cu/Al_2O_3$ shows increase in diesel and decrease in gasoline fractions compared to Co/Al_2O_3. The Ca-containing cobalt catalysts displayed decrease in wax selectivity and increase in gasoline and diesel fractions. The four catalysts produced fairly similar distribution of kerosene fraction.

Although the carbon number distribution of hydrocarbons was similar, the catalysts displayed different activities and dissimilarities in terms of gross product selectivity (Table 6). $Co–Cu/Al_2O_3$ had lowest activity and hydrocarbon selectivity among the catalysts. Using steadystate isotopic transient kinetic analysis (SSITKA), the same intrinsic activity has been reported for unpromoted Co/Al_2O_3 of Co particle size from 4 to 15 nm. This suggests that desorption of CH_x and OH_x intermediates constitutes the rate limiting elementary step for small Co particles < 6 nm, which leads to lower Time of Flight (TOF) of Co particles < 6 nm. Similar explanation may be invoked for the observed lower activity of the promoted catalysts compared to the unpromoted one. It appears that the presence of the promoters increases surface residence times of CH_x and OH_x intermediates at the expense of CO, thereby resulting in lower hydrocarbon formation on the promoted catalysts[36,37].

More than $> 98.7\%$ of non-gaseous product is oxygenate-rich aqueous product. Recently, Bui and de Klerk[38] have

also drawn attention to cobalt leaching via carboxylic acids produced during FT synthesis. They have explained that there is high tendency of cobalt leaching if these carboxylates are produced in substantial amount during FT synthesis, because the decomposition temperatures of C_1–C_5 carboxylates of cobalt (> 250°C) are higher than the operating temperature for a typical cobalt-based low-temperature FT process (~ 220°C). However, ICPOES analysis of the aqueous products obtained from the Co–Cu/Al_2O_3 showed no clear evidence of cobalt leaching. Recent reports by de la Osa *et al.*[10] indicate that Ca-promoted cobalt catalysts increase FT synthesis rate and C_{5+} selectivity in favour of C_{16}–C_{16} hydrocarbons. A contrary result is obtained in the present study. The difference may be due to effect of catalyst preparation condition. After cobalt impregnation, de la Osa *et al.*[10] calcined their catalysts at 550°C, however, in this study the catalysts were calcined at 350°C.

Conclusion

The present work examines adsorption behaviour of H_2 and CO on γ-alumina supported Co and Co–Cu-based catalysts. Ca-modification of γ-alumina leads to catalysts with enhanced CO adsorption but decreased H_2 adsorption capacities. Although presence of Ca enhanced CO adsorption, it did not translate into increased activity and C_{5+} selectivity of the catalyst. Nature of Ca-phase in the catalysts influenced its promotion effect on the catalysts. As opposed to 350°C used in this study, calcination/activation temperatures ≥ 550°C is required for a Ca-promoted catalyst. Co–Cu-based catalysts display higher H_2 adsorption capacity and higher CO desorption temperature. At the higher CO desorption temperature, there is a relative lowering of CO adsorbed. This observation is linked with the decoration effect of copper on cobalt particles and oxygenate selectivity of Co–Cu catalysts. All the catalysts displayed selectivity towards gasoline and diesel fractions and similar distribution of kerosene fraction.

1. de Almeida, P. and Silva, P. D., The peak of oil production – timings and market recognition. *Energy Policy*, 2009, **37**, 1267–1276.
2. James, O. O., Mesubi, A. M., Ako, T. C. and Maity, S., Increasing carbon utilization in Fischer–Tropsch synthesis using H_2-deficient or CO_2-rich syngas feeds. *Fuel Process. Technol.*, 2010, **91**, 136–144.
3. James, O. O., Chowdhury, B., Mesubi, A. M. and Maity, S., Reflections on chemistry of Fischer–Tropsch synthesis. *RSC Adv.*, 2012, **2**, 7347–7366.
4. Sirijaruphan, A., Horvath, A., Goodwin Jr, J. G. and Oukaci, R., Cobalt aluminate formation in alumina-supported cobalt catalysts: effects of cobalt reduction state and water vapor. *Catal. Lett.*, 2003, **91**, 89–94.
5. Chu, W., Chernavskii, P. A., Gengembre, L., Pankina, G. A., Fongarland, P. and Khodakov, A. Y., Cobalt species in promoted cobalt alumina-supported Fischer–Tropsch catalysts. *J. Catal.*, 2007, **252**, 215–230.
6. Morales, F. and Weckhuysen, B. M., Promotion effects in Co-based Fischer–Tropsch catalysis. *Catalysis*, 2006, **19**, 1–40.
7. Khodakov, A. Y., Chu, W. and Fongarland, P., Advances in the development of novel cobalt Fischer–Tropsch catalysts for synthesis of long-chain hydrocarbons and clean fuels. *Chem. Rev.*, 2007, **107**, 1692–1744.
8. Diehl, F. and Khodakov, A. Y., Promotion of cobalt Fischer–Tropsch catalysts with noble metals: a review. *Oil Gas Sci. Technol.*, 2009, **64**, 11–24.
9. Bao, A., Liew, K. and Li, J., Fischer–Tropsch synthesis on CaO-promoted Co/Al_2O_3 catalyst. *J. Mol. Catal. A: Chem.*, 2009, **304**, 47–51.
10. de la Osa, A. R., De Lucas, A., Romero, A., Valverde, J. L. and Sánchez, P., Fischer–Tropsch diesel production over calcium-promoted Co/alumina catalyst: effect of reaction conditions. *Fuels*, 2011, **90**, 1935–1945.
11. Vahid, M., Peyrovi, M. H., Islami, M. and Mehr, J. Y., Synthesis of higher alcohols from syngas over Cu-Co_2O_3/ZnO, Al_2O_3 catalyst. *Appl. Catal. A: Gen.*, 2005, **281**, 259–265.
12. Zhang, H.-B., Dong, X., Lin, G.-D., Lian, G. X.-L. and Li, H.-Y., Carbon nanotubepromoted Co–Cu catalyst for highly efficient synthesis of higher alcohols from syngas. *Chem. Commun.*, 2005, 5094–5096.
13. Yu, L., Zhang, S., Guo, X., Wang, D., Wang, S. and Wu, S., Influence of the addition of Pd and Cu to cobalt catalysts prepared by SMAT for F–T synthesis. *Cent. Eur. J. Chem.*, 2007, **5**, 144–155.
14. Jacobs, G., Ribeiro, M. C., Ma, W., Ji, Y., Khalid, S., Sumodjo, P. T. A. and Davis, B. H., Group 11 (Cu, Ag, Au) promotion of 15%Co/Al_2O_3 Fischer–Tropsch synthesis catalysts. *Appl. Catal. A: Gen.*, 2009, **361**, 137–151.
15. Wang, J., Chernavskii, P. A., Khodakov, A. Y. and Wang, Y., Structure and catalytic performance of alumina-supported copper–cobalt catalysts for carbon monoxide hydrogenation. *J. Catal.*, 2012, **286**, 51–61.
16. Tsai, Y.-T., Mo, X. and Goodwin Jr, J. G., The synthesis of hydrocarbons and oxygenates during CO hydrogenation on Co-CuZnO catalysts: analysis at the site level using multiproduct SSITKA. *J. Catal.*, 2012, **285**, 242–250.
17. Carrier, X., Marceau, E., Lambert, J.-F. and Che, M., Transformations of γ-alumina in aqueous suspensions: 1. Alumina chemical weathering studied as a function of pH. *J. Colloid Interface Sci.*, 2007, **308**, 429–437.
18. Trueba, M. and Trasatti, S. P., γ-Alumina as a support for catalysts: a review of fundamental aspects. *Eur. J. Inorg. Chem.*, 2005, **2005**(17), 3393–3403.
19. Ellis, P. R., James, D., Bishop, P. T., Casci, J. L., Lok, C. M. and Kelly, G. J., Synthesis of high surface area cobalt on-alumina catalysts by modification with organic compounds. In *Advances in Fischer–Tropsch Synthesis, Catalysts and Catalysis* (eds Davis, B. H. and Occelli, M. L.), Taylor and Francis Group, 2010, pp. 1–16.
20. Ha, K.-S., Jung, G.-I., Woo, M.-H., Jun, K.-W. and Bae, J. W., Effects of phosphorus and saccharide on size, shape, and reducibility of Fischer–Tropsch catalysts for slurry phase and fixed-bed reactions. *Appl. Catal. A: Gen.*, 2013, **453**, 358–369.
21. Ehrhardt, C., Gjikaj, M. and Brockner, W., Thermal decomposition of nitro compounds: preparation of anhydrous cobalt (II) nitrate and its characteristics by infrared and Raman spectra. *Thermochim. Acta*, 2005, **432**, 36–40.
22. Tüysüz, H., Liu, Y., Weidenthaler, C. and Schüth, F., Pseudomorphic transformation of highly ordered mesoporous Co_3O_4 to CoO via reduction with glycerol. *J. Am. Chem. Soc.*, 2008, **130**, 14108–14110.
23. Chernavskii, P. A., Pankina, G. V. and Lunin, V. V., The influence of oxide–oxide interaction on the catalytic properties of Co/Al_2O_3 in CO hydrogenation. *Catal. Lett.*, 2000, **66**, 121–124.

24. PeÂrez-RamõÂrez, J., Mul, G., Kapteijn, F. and Moulijn, J. A., *In situ* investigation of the thermal decomposition of Co–Al hydrotalcite in different atmospheres. *J. Mater. Chem.*, 2001, **11**, 821–830.
25. Tsyganenko, A. A. and Mardilovich, P. P., Structure of alumina surfaces. *J. Chem. Soc., Faraday Trans*., 1996, **92**, 4843–4852.
26. Gopalakrishnan, R. and Viswanathan, B., Interaction of CO and hydrogen on cobalt surfaces: a temperature-programmed desorption study. *Surf. Technol*., 1984, **23**, 173–177.
27. Gopalakrishnan, R. and Viswanathan, B., Temperature-programmed desorption and infrared studies on the activation of carbon monoxide on cobalt surfaces. *J. Colloid Interface Sci*., 1984, **102**, 370–372.
28. Mo, X., Tsai, Y.-T., Gao, J., Mao, D. and Goodwin Jr, J. G., Effect of component interaction on the activity of Co/CuZnO for CO hydrogenation. *J. Catal*., 2012, **285**, 208–215.
29. Sitthisa, S., Pham, T., Prasomsri, T., Sooknoi, T., Mallinson, R. G. and Resasco, D. E., Conversion of furfural and 2-methylpentanal on Pd/SiO_2 and Pd–Cu/SiO_2 catalysts. *J. Catal*., 2011, **280**, 17–27.
30. Reddy, B. M., Reddy, G. K., Rao, K. N., Khan, A. and Ganesh, I., Silica supported transition metal-based bimetallic catalysts for vapour phase selective hydrogenation of furfuraldehyde. *J. Mol. Catal. A: Chem.*, 2007, **265**, 276–282.
31. Sitthisa, S. and Resasco, D. E., Hydrodeoxygenation of furfural over supported metal catalysts: a comparative study of Cu, Pd and Ni. *Catal. Lett*., 2011, **141**, 784–791.
32. Shi, L., Chu, W. and Deng, S., Catalytic properties of Cu–Co catalysts supported on HNO_3-pretreated CNTs for higher-alcohol synthesis. *J. Nat. Gas Chem.*, 2011, **20**, 48–52.
33. Yang, X., Wei, Y., Su, Y. and Zhou, L., Characterization of fused Fe–Cu based catalyst for higher alcohols synthesis and DRIFTS investigation of TPSR. *Fuel Process. Technol*., 2010, **91**, 1168–1173.
34. Smith, M. L., Kumar, N. and Spivey, J. J., CO adsorption behaviour of Cu/SiO_2, Co/SiO_2, and CuCo/SiO_2 catalysts studied by *in situ* DRIFTS. *J. Phys. Chem. C*, 2012, **116**, 7931–7939.
35. Kollár, M., De Stefanis, A., Solt, H. E., Mihályi, M. R., Valyon, J. and Tomlinson, A. A. G., The mechanism of the Fischer–Tropsch reaction over supported cobalt catalysts. *J. Mol. Catal. A: Chem*., 2010, **333**, 37–45.
36. Yang, J., Tveten, E. Z., Chen, D. and Holmen, A., Understanding the effect of cobalt particle size on Fischer–Tropsch synthesis: surface species and mechanistic studies by SSITKA and kinetic isotope effect. *Langmuir*, 2010, **26**(21), 16558–16567.
37. den Breejen, J. P., Radstake, P. B., Bezemer, G. L., Bitter, J. H., Frøseth, V., Holmen, A. and de Jong, K. P., On the origin of the cobalt particle size effects in Fischer–Tropsch catalysis. *J. Am. Chem. Soc*., 2009, **131**(20), 7197–7203.
38. Bui, L. and de Klerk, A., Cobalt carboxylate stability and the implications for Fischer–Tropsch catalysis and syncrude refining; http://abstracts.acs.org/chem/243nm/program/view.php (accessed on 9 September 2012).

ACKNOWLEDGEMENTS. O.O.J. thanks TWAS, Trieste Italy, and CSIR, New Delhi for the award of TWAS–CSIR Postgraduate Fellowship. We thank Thermo Fisher (India) for assistance with analysis of the liquid hydrocarbons in this study.

Received 1 November 2013; revised accepted 15 April 2014

Smile with Science

By – Neelu Singh
e-mail: neelu.singh0387@gmail.com